



AUTHOR(S):

TITLE:

YEAR:

Publisher citation:

OpenAIR citation:

Publisher copyright statement:

This is the _____ version of an article originally published by _____
in _____
(ISSN _____; eISSN _____).

OpenAIR takedown statement:

Section 6 of the "Repository policy for OpenAIR @ RGU" (available from <http://www.rgu.ac.uk/staff-and-current-students/library/library-policies/repository-policies>) provides guidance on the criteria under which RGU will consider withdrawing material from OpenAIR. If you believe that this item is subject to any of these criteria, or for any other reason should not be held on OpenAIR, then please contact openair-help@rgu.ac.uk with the details of the item and the nature of your complaint.

This publication is distributed under a CC _____ license.

Zinc-Modified Nanotransporter of Anticancer Drugs for Targeted Therapy: Biophysical Analysis

Sylvie Skalickova¹, Michaela Docekalova¹, Martina Stankova¹, Dagmar Uhlířova¹,
Branislav Ruttkay-Nedecký¹, Carlos Fernandez², Marta Kepinska³,
Halina Milnerowicz³, and Rene Kizek^{1,3,*}

¹Central Laboratory, Faculty of Pharmacy, University of Veterinary and Pharmaceutical Sciences Brno,
Palackého 1941/1 Brno, Czech Republic

²School of Pharmacy and Life Sciences, Robert Gordon University, Aberdeen AB107GJ, United Kingdom

³Wrocław Medical University, Department of Biomedical and Environmental Analyses,
Ludwika Pasteura 1, 50-367 Wrocław, Poland

Modern anticancer therapy aims to increase the effectiveness of tumor treatment. The aim of this work was to propose a new nanotransporter for targeted delivery of anthracycline antibiotics, which is characterized by its bioavailability, increased uptake of the drug from the bloodstream at the site of tumor tissue and as well as low toxicity to non-target tissue. Chitosan nanoparticles have attracted great attention in the field of drug delivery due to their stability, low toxicity and easy preparation. Deacetylated chitosan skeleton is composed of glucosamine units and has a high density of charged amino groups which allow strong electrostatic interactions with biomolecules, transition metals (Zn, Se) and peptides. We obtained the encapsulation effectiveness of chitosan 20%. Electrochemical detection of the bounded Zn²⁺ ions into the chitosan structure showed shift from -0.99 to -0.93 V. This result proved the formation of a chitosan-zinc complex. The ability of metallothionein to quench the 2,2-diphenyl-1-picrylhydrazyl radical in the presence of 50 μ M doxorubicin was confirmed by the change of relative absorbance in the range of 50 to 60%.

Keywords: Breast Cancer, Chitosan, Doxorubicin, Nanoparticles, Zinc.

1. INTRODUCTION

The conventional treatment of malignant tumors include local ways such as surgery, radiotherapy with the combination of chemotherapy, hormone therapy and biological treatment.¹ For oncological patients with metastasis is the most used chemotherapeutic doxorubicin (DOX).² Treatment response is in the range of 25% and 33%, with a median progression of 3.6 months and a median survival of 8.9 months. Despite DOX therapeutic efficacy it exhibits high cardiotoxicity.³ This side effect limits the cumulative applied dose. Heart muscle damage is reported in 3% of patients at 400 mg/m², 7% at 500 mg/m², and in more than 15% of patients heart damage at 700 mg/m².⁴

The development of new type of nanotransporter is focused on the decrease of DOX induced cardiotoxicity. Several nanotechnological approaches have been successfully used for the decrease of side effects induced

by various anthracycline antibiotics utilized for hematological malignancies and solid tumors therapy.^{5,6} The nanotransporter modification of therapeutics allows its targeting preferentially to cancer cell and moreover could increase level of anticancer drug in the final destination without increasing the side effects. Additionally, drugs closed in a nano-cage are protected from intracellular enzymatic degradation or endosomal translocation. Recently, chitosan nanoparticles have gained more attention due to their stability, low toxicity and simple preparation in the field of targeted drug transport.⁷ Deacetylated chitosan backbone of glucosamine clusters shows high electrostatic interactions with biomolecules, metals (Zn, Se) and/or peptides.^{8,9}

It is generally known that metallothionein (MT) is a metal-binding protein responsible for zinc homeostasis and heavy metal detoxification in the organism. In our previous published work, we showed the significant increase of MT in malignant tumors.^{10–12} Furthermore, it has been

*Author to whom correspondence should be addressed.

estimated that the MT level in breast cancer significantly increase due to higher metabolic activity of the tumor tissue and defense system against oxidative stress induced by chemotherapeutics.^{13–15}

The aim of our study was to design a chitosan based nanotransporter for DOX which was modified by zinc ions (Zn-ChNPs-DOX). Zinc ions were involved for higher uptake from the bloodstream via interaction with MT. We suppose the free –SH groups of MT bind preferentially to the structure of Zn-ChNPs-DOX. In the experiment, chitosan nanotransporter was designed and subsequently studied by biophysical methods.

2. EXPERIMENTAL DETAILS

2.1. Chemicals

Doxorubicin, chitosan, zinc chloride, metallothionein in II from rabbit liver, ssDNA (AGGATCTGATCC) ACS water and other chemicals were purchased from Sigma-Aldrich (St. Louis, USA) in ACS purity unless noted otherwise.

2.2. Chitosan Nanoparticles Preparation

12.5 mg of low MW chitosan was dissolved in 5 mL of 3% acetic acid. DOX (30 μ M) was added to the chitosan solution under stirring (3 hours, 24 °C). After DOX dissolution, the sodium tripolyphosphate (0.25% w/v) was added dropwise. The unbound DOX was removed using centrifugation procedure. The solution was transferred in to the tubes and centrifuged 10 min, 14000 rpm (Eppendorf centrifuge, Hamburg, Germany). The pellet was dissolved in 5 mL of 3% acetic acid.

2.3. Preparation of Chitosan Nanoparticles with Encapsulated DOX Modified by Zinc

ZnCl₂ was added to chitosan nanoparticles (ChNPs) with encapsulated DOX at a final ZnCl₂ concentration of 1.0 mM. The solution was stirred for 30 min before use.

2.4. Electrochemical Determination of Zinc Ions

Determination of Zn²⁺ by difference pulse voltammetry (DPV) was performed at 663 VA Stand (Metrohm, Switzerland) connected with AUTOLAB Analyzer (Metrohm-Autolab B.V., Utrecht, The Netherlands). Adsorptive transfer technique and a standard cell with three electrodes was used for measurement. A hanging mercury drop electrode (HMDE) with a drop area of 0.4 mm² was employed as the working electrode. An Ag/AgCl/3 M KCl electrode acted as the reference and platinum electrode was auxiliary. For data processing NOVA software (Metrohm, Utrecht, The Netherlands) was employed. The analyzed samples were deoxygenated prior to measurements by purging with argon (99.999%). Acetate buffer (0.2 M sodium acetate and 0.2 M acetic acid, pH = 5) was used as a supporting electrolyte. The parameters of the measurement were as follows: initial potential 0 V, end potential –1.7 V, deoxygenating with

argon 30 s, accumulation time 120 s, step potential 5 mV, modulation amplitude 25 mV, volume of injected sample 5 μ L, volume of measurement cell 2 mL (5 μ L of sample and 1995 μ L supporting buffer).

2.5. Fluorometric and Spectroscopic Measurements of Doxorubicin

Fluorescence spectra were acquired by a multifunctional microplate reader Tecan Infinite 200 PRO (TECAN, Switzerland). Excitation wavelength for DOX was 480 nm. The fluorescence scan of DOX was measured within the range from 510–850 nm per 2-nm steps. The detector gain was set to 100. Absorbance of ssDNA was measured at λ = 260 nm. Each absorbance value is an average of three measurements. The samples for measurements (2 μ L) were placed in 96 well plate by Tecan (TECAN, Switzerland). All measurements were performed at 25 °C controlled by the Tecan Infinite 200 PRO (TECAN, Switzerland).

2.6. Metallothionein Scavenging of the Free Radicals

Spectrophotometric measurements of 2,2-diphenyl-1-picrylhydrazyl (DPPH) were carried out using an automated chemical analyser BS-200 (Mindray, Shenzhen, China). Reagents and samples were placed on cooled sample holder (4 \pm 1 °C) and automatically pipetted directly into plastic cuvettes. Incubation proceeded at 37.0 \pm 0.1 °C. Mixture was consequently stirred. The washing steps of pipetting needle with distilled water (18 m Ω) were done during the pipetting. For detection itself, the following range of wavelengths were used—340, 380, 412, 450, 505, 546, 570, 605, 660, 700, 740 and 800 nm. The instrument was operated using the BS-200 software (Mindray, Shenzhen, China).

The DPPH test is based on the ability of the stable DPPH free radical to react with hydrogen donors. The DPPH[•] radical displays an intense UV-VIS absorption spectrum. In this test, a solution of radical is decolorized after reduction with antioxidant (AH) or a radical (R[•]) in accordance with the following scheme: DPPH[•] + AH \rightarrow DPPH-H + A[•], DPPH[•] + R[•] \rightarrow DPPH-R. 150 μ L of DPPH reagent was pipetted into a plastic cuvette. Subsequently, 15 μ L of sample was added to the solution. DPPH conducts a strong absorption in the UV-VIS spectrum, absorbance was measured for 12 min at λ = 505 nm. To assess the production of free radicals, the absorbance difference of the reagent without sample and reagent with sample after ten-minute incubation was taken. After subtraction of the blank value the biggest absorbance difference was taken as 100% of the amount of free radicals. The higher the amount of free radicals was, the higher was the oxidative stress.

2.7. Ellman Assay

For analysis of thiol groups was used an Ellman spectrophotometric assay. 277 μ L of Ellman reagent (R1)

(2 mM 5,5'-dithiobis(2-nitrobenzoic acid) in 2 mM $\text{Na}_2(\text{CH}_3\text{COO}_2)$) was pipetted in the cuvette, subsequently the 45 μL of sample and 33 μL of reagent (R2) (1 M CH_3COOH) were added to the mixture. The mixture was incubated for 10 min at 37 °C. The absorbance was recorded at 405 nm. The Ellman assay was carried out using an automated chemical analyser BS-200 (Mindray, Shenzhen, China). Reagents and samples were placed on a cooled sample holder (4 ± 1 °C) and automatically pipetted directly into the plastic cuvettes. Incubation proceeded at 37.0 ± 0.1 °C. Mixture was consequently stirred. The washing steps of pipetting needle with distilled water (18 m Ω) were done during the pipetting. The instrument was operated using the BS-200 software (Mindray, Shenzhen, China).

2.8. Descriptive Statistics

Data were processed using MICROSOFT EXCEL® (USA). Results are expressed as mean \pm standard deviation (S.D.) unless noted otherwise.

3. RESULTS AND DISCUSSION

The unique properties of chitosan were employed for DOX delivery to the target tissue with the utilization of zinc ions. The DOX encapsulation by chitosan polymeric cage decorated by Zn^{2+} via electrostatic interaction is shown in Figure 1. The formation of the chitosan nanoparticles and its interaction with metallothionein in is further biophysically examined.

3.1. Chitosan Nanoparticles Characterization

We used size measurement and Z-potential characterization of colloidal state of the nanoparticle system in our experiment. Figure 2(A) demonstrated that size of the nanoparticles was found to be 40 ± 3 nm. Measurement

of the Z-potential (or charge density) provides important information about predicting their binding capacity. We confirmed that chitosan nanoparticles carry positive charge approximately of 50 mV. We tested the dependence of tripolyphosphine (TPP) addition on Z-potential of the formed nanoparticles. Figure 2(B) shows that the highest Z-potential is caused by 0.0025 μM addition of TPP. The higher TPP addition causes a decrease of the Z-potential. This effect could be explained due to the accumulation of counterions near the surface causing charges and subsequently reducing the Z-potential.

3.2. Zinc Binding to the Structure of ChNPs

Electrochemical measurement was used due to its sensitivity and ability to monitor the course of interactions. Figure 2(C) shows a characteristic peak of Zn^{2+} with the potential about -1.0 V. Although, chitosan alone does not exhibit electrochemical activity and after interaction with zinc ions the electrochemical signal shifts to more positive potential. Simultaneously, the additional electrochemical signal occurs at the potential about -0.2 V depending on the zinc concentration. This result could be explained by the formation of a zinc-chitosan complex. The dependence of potential and electrochemical signal on zinc concentration is summarized in the graph Figure 2(D). From the obtained data we could conclude that the higher concentration of chitosan caused a decrease in the electrochemical signal of zinc up to a concentration of 300 $\mu\text{g}/\text{mL}$. Therefore, higher concentrations of chitosan do not have an effect on the zinc electrochemical signal. Simultaneously, we observed that the higher concentration of chitosan shifts zinc electrochemical potential from -0.99 to -0.93 V. In summary, our results confirmed the formation of a chitosan-zinc complex. Considering the fact, that chitosan is used for electrode coating, especially in biosensors, the observed interaction course is consistent with other published work.¹⁶

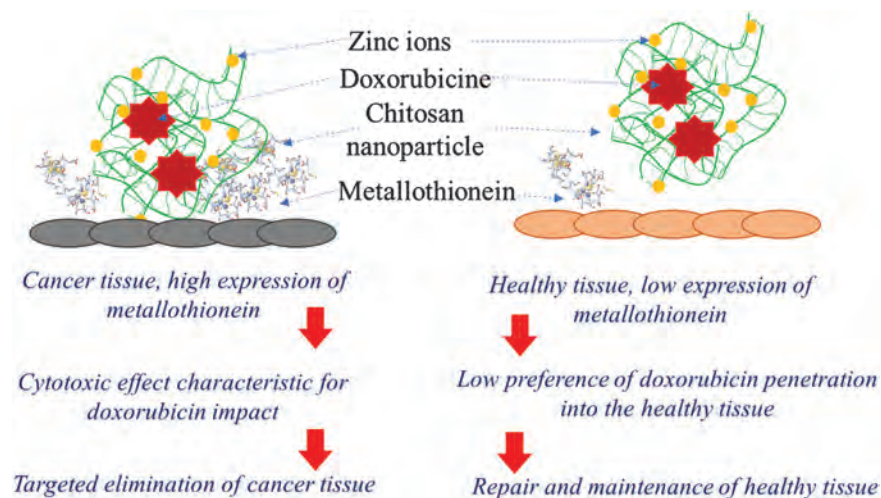


Figure 1. Simplified scheme of chitosan nanotransporter focused on tumor tissue. Cancer cells highly express molecules of metallothionein in the comparison with a healthy tissue.²¹ Designed nanotransporter Zn-ChNPs-DOX preferentially binds into the active metallothionein clusters.

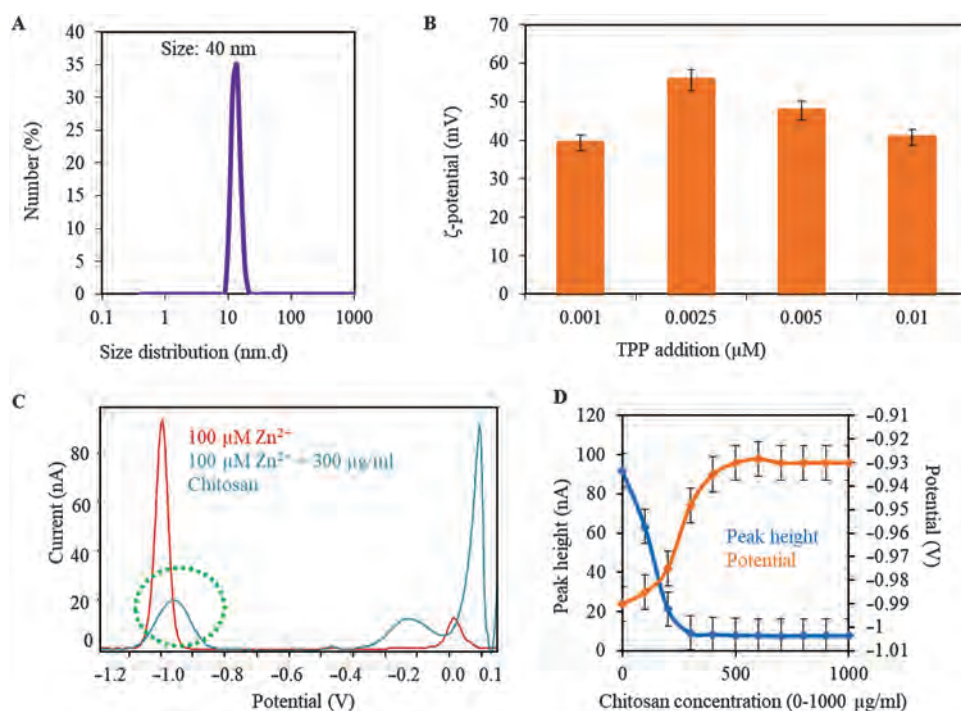


Figure 2. (A) The size distribution of the ChNP-DOX (0.5 μM DOX, 0.0025 μM TPP). MilliQ water was used as the solvent. (B) Dependence of TPP addition (0.001–0.01 μM) on ChNP-DOX Z-potential. (C) Zinc at a concentration of 100 μM was titrated with 100 $\mu\text{g/ml}$ chitosan. (D) Dependence of peak height and potential on chitosan concentration (0–1000 $\mu\text{g/ml}$) for the complex formation. Measurement was carried out in acetate buffer, pH 5.0, DPV with a 90 s accumulation time.

3.3. Doxorubicin Encapsulation

We involved a fluorescence as a suitable analytical tool for characterization and determination the encapsulation efficiency of chitosan nanoparticles. 3 μM DOX shows 9% quantum yield which enables the sensitive detection.¹⁷

Firstly, the dependence of fluorescence signal on DOX concentration was evaluated. The obtained calibration curve shows a linear trend in the concentration range from 0 to 30 μM with the following linear equation: $y = 1601.2x + 2012.3$ and $R^2 = 0.9944$ (Fig. 3(A)). The limit of DOX fluorometric detection was found to be 0.09 μM (3 S/N). For the determination of the encapsulation efficiency, the doxorubicin itself (30 μM) and encapsulated DOX (DOX-ChNPs) fluorescence intensity was compared. The decrease of the fluorescence intensity for DOX-ChNPs could be observed from the emission spectra (Fig. 3(B)). The concentration of an encapsulated DOX was calculated to be 6 μM which corresponds to 20% encapsulation effectivity.

The goal of our study was to encapsulate DOX into chitosan nanoparticles and to minimize the number of molecules on the nanoparticles surface. We took the advantage of DOX intercalation ability into the structure of DNA to determine the presence of DOX (30 μM) on ChNPs surface. The intercalated DOX into the (1 mM) DNA showed a significant decrease of the fluorescence signal (Fig. 3(C), on top). Consequently, the DOX-ChNPs was analyzed before and after the purification step which

removes unbound DOX. The obtained results demonstrated a higher fluorescence signal for the unpurified DOX-ChNPs which could be explained due to the removal of unbound DOX. In the presence of DNA, the fluorescence signal decrease occurs in both cases. To evaluate the changes of fluorescence signals the size of the difference was calculated before and after purification of ChNP-DOX. The higher decrease of the fluorescence signal was estimated in the case of unpurified DOX-ChNPs which means that DOX appears on the surface of the nanoparticles at low concentration. Obtained results are in good agreement with other studies based on the doxorubicin-chitosan nanoparticle formation.^{18–20} Our approach excels in the simplicity and availability of the experimental design.

3.4. ChNPs-DOX Interaction with MT

One proposed mechanism of action of DOX after its metabolism is the formation of a number of radicals, which lead to a cell damage and later to apoptosis. In several malignant tumors there is a significant increase of thiol levels (explained by the increase of MT synthesis), that presumably scavenge molecules used for damaging the tumor cells. Due to this effect, the tumor cell resistance for the used cytostatic increases. In our study, we aimed to assess the effect of thiols capable of capturing the radicals, especially MT. To date, very little attention has been paid to this issue and mechanisms of these interactions have not

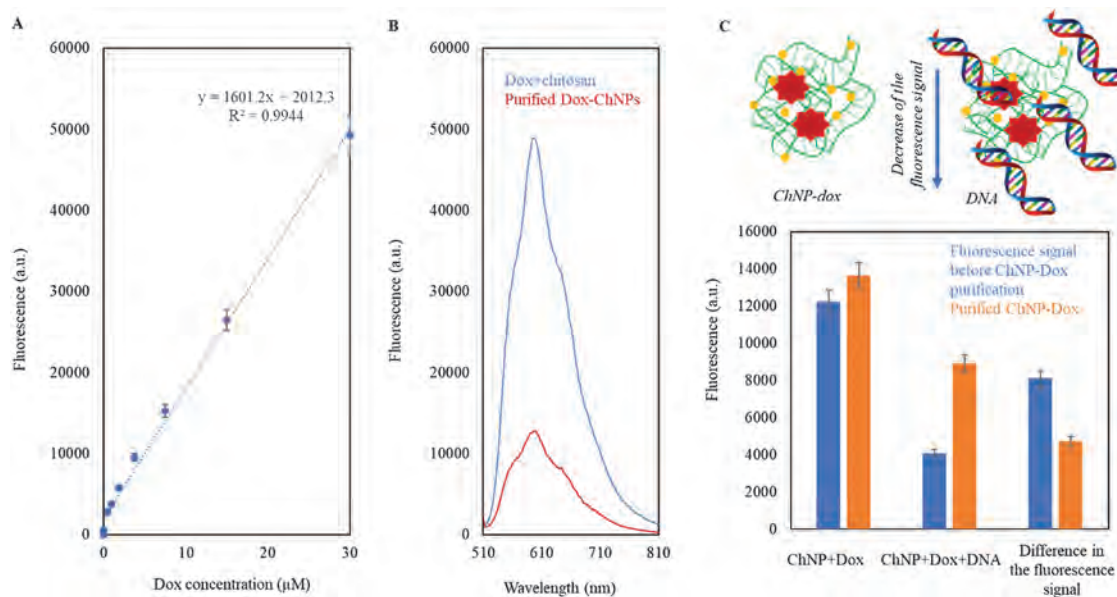


Figure 3. (A) Dependence of doxorubicin concentration (0–30 μM) on fluorescence signal. (B) Difference in emission wavelengths of DOX-chitosan (doxorubicin concentration 30 μM) and purified DOX-ChNPs. (C) Characterization of DOX (6 μM) position on the crosslinked nanoparticle using DNA.

been described yet. In this experiment, DPPH radical was used.

Figure 4(A) shows the effect of DOX added to the DPPH reaction mixture at different concentrations. The observed signals are within a 10% deviation due to a laboratory error, and the resultant DPPH signal does not change at any of the tested doxorubicin concentrations. MT (1000 $\mu\text{g/mL}$) scavenged the DPPH radical very intensively (signal change by more than 200%), see Figure 4(B). In case that DOX was added to the MT,

the progressive blocking of the -SH groups for Ellman's reagent (Fig. 4(B), grey bars) was observed with the increase of the DOX concentration, and after 100 μM addition of DOX the resulting MT signal change was more than 100%.

The results indicate the considerable ability of MT to quench the DPPH radical in the presence of 50 μM DOX, the signal change was found to be between 50–60%. Figure 4(C) shows the effect of different amounts of MT and its ability to quench the DPPH radical. The result

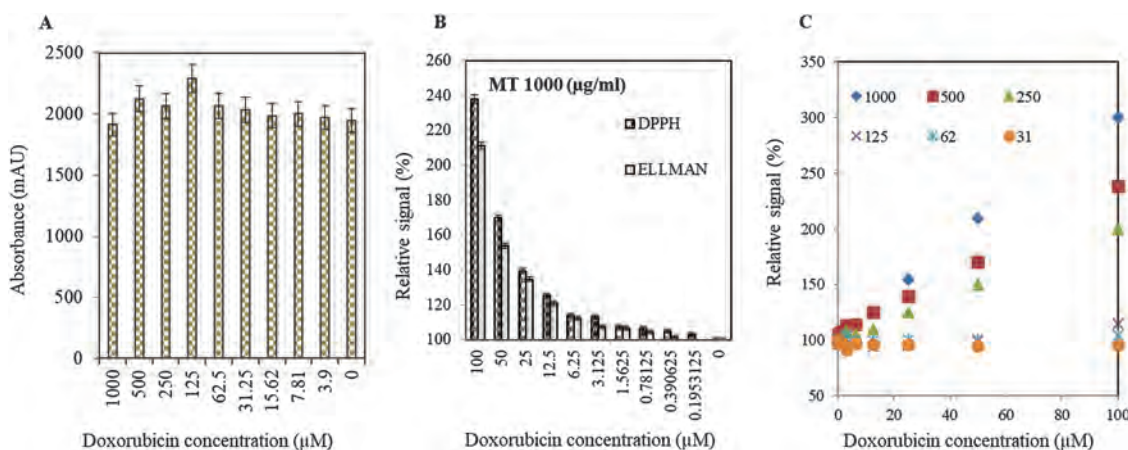


Figure 4. Interaction study of DOX with MT in the assessment of the capacity to scavenge DPPH radical. (A) Effect of DOX at defined concentrations (0, 1.9, 3.9, 7.8, 15.6, 31.2, 62.5, 125, 250, 500 and 1000 μM) on the resulting signal. (B) Addition of MT (1000 $\mu\text{g/mL}$) to the DPPH radical in the presence of defined concentrations of DOX, free -SH of the thiol group were analysed by the Ellman method (405 nm). (C) Changes in the DPPH radical signal in the presence of defined DOX concentrations and 1000, 500, 250, 125, 62 and 31 $\mu\text{g/mL}$ MT. The interaction study was performed immediately after mixing DOX and MT (1:1) in an automatic mode (5 μL of sample) at 37 $^{\circ}\text{C}$. The results were evaluated from the reaction curve and recalculated to a relative signal, where 100% was always a DPPH with MT. The relative changes of the DPPH signal were determined by the photometric method (537 nm), see Material and Methods for further details.

clearly demonstrated the notable ability of thiol compounds to react with radical molecules and thus reduce the effectiveness of antitumor treatment (1 μg of MT reacts with DPPH by changing the signal by 0.2145). For these reasons, it is necessary to look for suitable tools to overcome this natural biological base of resistance.

4. CONCLUSION

To the conclusion, new nanotransporter is characterized by its bioavailability, increased uptake of drug from the blood stream at the site of tumor tissue, and low toxicity to non-targeted tissues. The results showed that the chitosan nanoparticle closes DOX in its structure and Zn^{2+} ions are bound to its surface. DOX-ChNPs of size 40 nm were successfully designed. The fluorescence quenching effect of doxorubicin was used for the evaluation of non-encapsulated DOX molecules on the nanoparticle surface. The results demonstrated the formation of chitosan nanoparticles and their ability to bind on the MT protein, which plays an important role in the breast cancer.

Acknowledgments: Projects Liga Proti Rakovině Praha 2017, NANODRUGS328/2017/FaFand the European Technology Platform for Nanomedicine.

References and Notes

1. P. V. Viscuse, K. Price, D. Millstine, A. Bhagra, B. Bauer, and K. J. Ruddy, *Current Opin. Oncol.* 29, 235 (2017).
2. M. L. Schirinzi, O. Poti, D. De Giorgi, C. Olla, S. Mancarella, and G. De Maria, *Ann. Oncol.* 27, 76 (2016).
3. S. Shabalala, J. Louw, C. Muller, and R. Johnson, *Life Sci.* 180, 160 (2017).
4. S. R. Jean, D. V. Tulumello, C. Riganti, S. U. Liyanage, A. D. Schimmer, and S. O. Kelley, *ACS Chem. Biol.* 10, 2007 (2015).
5. J. J. Shi, P. W. Kantoff, R. Wooster, and O. C. Farokhzad, *Nat. Rev. Cancer* 17, 20 (2017).
6. Z. Yaari, D. da Silva, A. Zinger, E. Goldman, A. Kajal, R. Tshuva, E. Barak, N. Dahan, D. Hershkovitz, M. Goldfeder, J. S. Roitman, and A. Schroeder, *Nat. Commun.* 7, 13325 (2016).
7. N. Kamaly, J. C. He, D. A. Ausiello, and O. C. Farokhzad, *Nat. Rev. Nephrol.* 12, 738 (2016).
8. H. Y. Zhao, P. Lv, D. Huo, C. Zhang, Y. Ding, P. P. Xu, and Y. Hu, *RSC Adv.* 5, 60549 (2015).
9. A. Esmaeili and N. A. Hadad, *Ceram. Int.* 41, 7529 (2015).
10. J. Gumulec, M. Masarik, V. Adam, T. Eckschlager, I. Provaznik, and R. Kizek, *PLoS One* 9, e99790 (2014).
11. J. Gumulec, M. Raudenska, V. Adam, R. Kizek, and M. Masarik, *PLoS One* 9, e85346 (2014).
12. V. Adam, J. Petrlova, J. Wang, T. Eckschlager, L. Trnkova, and R. Kizek, *PLoS One* 5, e11441 (2010).
13. A. Gomulkiewicz, K. Jablonska, B. Pula, J. Grzegorzolka, S. Borska, M. Podhorska-Okolow, A. Wojnar, J. Rys, A. Ambicka, M. Ugorski, M. Zabel, and P. Dziegiel, *Int. J. Oncol.* 49, 2487 (2016).
14. C. Burton, Y. B. Dan, A. Donovan, K. Liu, H. L. Shi, Y. F. Ma, and C. P. Bosnak, *Clin. Chim. Acta* 452, 142 (2016).
15. P. Chandler, B. S. Kochupurakkal, S. Alam, A. L. Richardson, D. I. Soybel, and S. L. Kelleher, *Mol. Cancer* 15, 2 (2016).
16. C. Petchthanasombat, T. Tiensing, and P. Sunintaboon, *J. Colloid Interface Sci.* 369, 52 (2012).
17. N. S. H. Motlagh, P. Parvin, F. Ghasemi, and F. Atyabi, *Biomed. Opt. Express* 7, 2400 (2016).
18. M. A. Raja, M. Arif, C. Feng, S. Zeenat, and C. G. Liu, *J. Biomater. Appl.* 31, 1182 (2017).
19. P. I. P. Soares, A. I. Sousa, J. C. Silva, I. M. M. Ferreira, C. M. M. Novo, and J. P. Borges, *Carbohydr. Polym.* 147, 304 (2016).
20. G. D. Souto, Z. Farhane, A. Casey, E. Efeoglu, J. McIntyre, and H. J. Byrne, *Anal. Bioanal. Chem.* 408, 5443 (2016).
21. B. Wierzowiecka, A. Gomulkiewicz, L. Cwynar-Zajac, M. Olbromski, J. Grzegorzolka, C. Kobierzycki, M. Podhorska-Okolow, and P. Dziegiel, *In Vivo* 30, 271 (2016).

Received: 13 June 2017. Accepted: 4 October 2017.